World Academy of Science, Engineering and Technology
International Journal of Materials and Metallurgical Engineering
Vol:10, No:5, 2016

Plasma Spraying of 316 Stainless Steel on Aluminum and Investigation of Coat/Substrate Interface

P. Abachi, T. W. Coyle, P. S. Musavi Gharavi

Abstract**—**By applying coating onto a structural component, the corrosion and/or wear resistance requirements of the surface can be fulfilled. Since the layer adhesion of the coating influences the mechanical integrity of the coat/substrate interface during the service time, it should be examined accurately. At the present work, the tensile bonding strength of the 316 stainless steel plasma sprayed coating on aluminum substrate was determined by using tensile adhesion test, TAT, specimen. The interfacial fracture toughness was specified using four-point bend specimen containing a saw notch and modified chevron-notched short-bar (SB) specimen. The coating microstructure and fractured specimen surface were examined by using scanning electron- and optical-microscopy. The investigation of coated surface after tensile adhesion test indicates that the failure mechanism is mostly cohesive and rarely adhesive type. The calculated value of critical strain energy release rate proposes relatively good interface status. It seems that four-point bending test offers a potentially more sensitive means for evaluation of mechanical integrity of coating/substrate interfaces than is possible with the tensile test. The fracture toughness value reported for the modified chevron-notched short-bar specimen testing cannot be taken as absolute value because its calculation is based on the minimum stress intensity coefficient value which has been suggested for the fracture toughness determination of homogeneous parts in the ASTM E1304-97 standard.

Keywords**—**Bonding strength, four-point bend test, interfacial fracture toughness, modified chevron-notched short-bar specimen, plasma sprayed coating.

I. Introduction

PLASMA spray, owing to some benefits such as possibility to use almost any coating material, locally limited and/or large coating area on the component has gained considerable attention as viable coating process [1], [2]. The plasma sprayed coatings are widely used in automotive, airplane, oil and chemical industries to produce oxidation, corrosion and wear resistant surface. The Volkswagen (VW) company has firstly mass produced Lupo FSI engine with the plasma spray coated cylinder surface [3], [4]. In spite of advantages, this coating method suffers from some inherent disadvantages, including porosity due to gas entrapment, oxidation of the coatings sprayed in air, solidification and cooling shrinkages, as well as, thermal residual stresses. The coating is subjected to the tensile force, and substrate is in compression state after the impact of the spraying particles on the substrate surface. Since such thermal stresses lower the adhesive strength of the layer, the maximum permissible layer thickness is often limited [5]. Certainly, mechanical performance and integrity of the interface are influenced by some parameters such as the thermal residual stresses, elastic mismatch of coating and substrate, plastic flow of the ductile component, defects in coating and interfaces [6]. These parameters are, in turn, affected by coating process and material's combination. For quality control of coating and optimization of the coating process, the adhesion between coating and substrate should be investigated. For this purpose, there are some approaches which are investigated by researchers [7]-[13]. In this work, it has been tried to examine three kinds of methods.

A. Theoretical Background

1. Examination of Tensile Bonding Strength

In spite of simplicity and popularity of standard tensile adhesive test (TAT) corresponding with ASTM C633, the method suffers from some limitations such as necessity to repeat each test for five times, need to use adhesive and probability of adhesive penetration to coat, low sensitivity for material defects like micro-cracks, voids, oxidation of splats interfaces during processing and inclusion in coatings [14]. However, these defects cause stress concentration and weaken the adhesive linkage inside the coating system. Referring to Qian et al. [12] statements, TAT, which is based on defect free assumption, overestimates the adhesive capacity of a practical coating system. There are also further shortcomings with TAT such as large differences between stress state of coatings in test and service conditions, difficulties in explanation of tests results when failure occurs in a combination of the locations (within coating plus coating-substrate interface) [15]. Although, this test is the most common method used to determine the adhesion level of a coating to its substrate, it is recommended for quality control and developing thermal spray coatings with improvement adhesion and integrity [14].

2. Evaluation of Interfacial Fracture Toughness; Using Four-Point Bending Test Specimen

The fracture toughness approach involving determination of fracture energy release rate, G_{ss}, and stress intensity factor, K_c, of coating based on the compliance calibration method of linear elastic fracture mechanics could be more proper to characterize the adhesion of coating to substrate and

P. Abachi is now with Center for Advanced Coating Technologies, University of Toronto, Toronto-Canada and former was with Sharif University of Technology, Dept. of Mater. Sci. and Eng. Tehran, Iran (corresponding author; phone: 416-946-0507; e-mails: abapar1056@gmail.com, p.abachi@utoronto.ca).

T. W. Coyle is with Center for Advanced Coating Technologies, University of Toronto, Toronto-Canada (e-mail: tom.coyle@utoronto.ca).

P. S. Musavi Gharavi is PhD Student at Department of. of Mater. Sci. and Eng., University of New South Wales, Sydney, Australia (e-mail: p.musavigharavi@student.unsw.edu.au).

satisfactory method for qualitative evaluation of coating failure [11], [16]-[20].

The four-point flexure test is based on the storage of a specific amount of elastic energy on bending and a release of this energy on fracture. Therefore, interfacial crack propagation occurs when the strain energy release rate, G_{ss}, equals to the critical energy release rate, G_c, of the interfacial failure. The critical energy release rate is calculated based on the assumptions made in linear elastic fracture mechanics and standard equations of LEFM [20]. This is valid when the plastic zone around the crack tip is very small. Some researchers have examined this method for analyzing the interface of different coating/substrate systems [5], [7], [8], [19].

Since, the strain energy release rate is independent of crack length, hence, the interfacial fracture energy can be determined using easily measurable parameters. During the test, specimen undergoes bending as well as tension. Consequently, mixed mode of fracture is expected [20]. In addition, due to fixed ends of the specimen during four-point bend test, the plane strain condition prevails. The constant bending moment, M, in the region between rollers is expressed as follows [20]:

$$M = \frac{FL}{2W} \tag{1}$$

where F is the critical load corresponding to delamination, W is the width of the specimen, and L is the distance between outer and inner rollers.

The strain energy release rate for a coated beam can be approximated as:

$$G_{ss} = \frac{18M^2(1-\nu_2^2)E_1}{(1-\nu_1^2)E_2^2}\frac{h_1}{h^4} \tag{2}$$

where, E_1 and E_2 represent the elastic modulus of the coating and the substrate, respectively. ν_1 and ν_2 are Poisson's ratio of the coating and substrate. h_1 and h_2 are the thickness of the coating and the substrate, correspondingly, when the total specimen's thickness equals h. Since, $h_1 << h_2$, h can be estimated as h_2.

Interfacial crack propagation occurs when the strain energy release rate, G_{ss}, equals the critical energy release rate, G_c, of the interfacial failure [21]:

$$G_c = \left(\frac{1}{\bar{E}_1} + \frac{1}{\bar{E}_2}\right)|K|^2/(2cosh^2\pi\varepsilon) \tag{3}$$

where K is stress intensity factor and

$$\bar{E}_i = E_i/(1-\nu_i^2) \tag{4}$$

for plane strain condition, E_i is Young's modulus and

$$cosh^2\pi\varepsilon = \frac{1}{1-\beta^2} \tag{5}$$

where ε is oscillation coefficient and can be represented as [22],

$$\varepsilon = \frac{1}{2\pi} ln\frac{1-\beta}{1+\beta} \tag{6}$$

with the Dundurs' parameter, β, as a measure of the mismatch in the in-plane bulk modulus [23]:

$$\beta = \frac{1}{2}\frac{\mu_1(1-2\nu_2)-\mu_2(1-2\nu_1)}{\mu_1(1-\nu_2)+\mu_2(1-\nu_1)} \tag{7}$$

For a stable crack at the interface, the stress intensity factor is defined as a complex form by stress fields near the crack tip as follows [22], [23]:

$$K = K_{1+}iK_2 = \lim_{r\to 0}\sqrt{2\pi}(\sigma_y + i\tau\sigma_{xy})/\, r^{i\varepsilon} \tag{8}$$

where μ_i and ν_i are shear modulus and Poisson's ratio, respectively, of material i (i = 1, 2) between which the interface exists. Subscriptions 1 and 2 refer to the related mechanical properties of coating and substrate, correspondingly. It is noted that K_1 and K_2 in the complex stress intensity factor K do not correspond to K_I of mode I and K_{II} of mode II, respectively. The growth of the interfacial crack can be described by a criterion expressed in term of the stress intensity factor or the strain energy release rate [21].

Generally, the value of fracture toughness in literature is quoted for mode I failure. In this way, the stress at the crack tip can be characterized by the stress intensity factor K. The failure occurs by crack growth when K reaches to a critical value K_{IC} [8], [24]:

$$K_{IC}^2 = \frac{G_c E}{(1-\nu^2)} \tag{9}$$

However, at the present study, the value of fracture toughness for mixed mode of failure has been presented.

3. Evaluation of Interfacial Fracture Toughness; Using Modified Chevron-Notched Short-Bar (SB) Specimen

For fracture toughness testing of ceramics, high-strength metals, and other brittle materials, Barker and other researchers [25]-[30] proposed short-rod and short-bar designs. Later, Mecholsky and Barker [31] developed a method of using the chevron-notch specimens to measure the interfacial toughness of ceramic-metal interfaces. Filiaggi and Pilliar [15] have also developed a convenient and reliable test method to assess the fracture toughness of ceramic-metal interface by modifying an existing homogeneous short-bar configuration. These Chevron-notched specimens have advantages over traditional fracture toughness specimens. The applied load leads to extensive stress concentrations at the tip of the chevron notch and, subsequently, to crack initiation at chevron notch. Therefore, there is no need of pre-cracking. Because of special geometry of the chevron notch, the crack advances stably. The long stable crack growth under mode I fracture mechanism, small specimen size and prevailing plane strain condition are the other advantages of this method [32]. Unstable crack growth occurs at a maximum load corresponding to a crack length, a, which is the function of the specimen geometry only. Fracture toughness can be evaluated

from the maximum load. There is no need to load-displacement plot, and the measurement of crack length is not required [32]. Therefore, the measurement of the critical value of the stress intensity factor can be performed on the same specimen for different lengths of a growing crack [33].

Alike to critical stress intensity factor (K_{ICSB}) determination for a homogeneous short-bar, assuming linear elastic behavior, the interfacial fracture toughness can be derived from the following equation [25]:

$$K_{IC} = \frac{Y_m^* P_{max}}{B\sqrt{W}} \quad (10)$$

where K_{IC} is the fracture toughness, and P_{max} is the maximum load to failure. Y_m^* is the minimum stress intensity coefficient. According to ASTM E1304, the dimensionless minimum stress intensity coefficient for homogeneous short-bar standard scaled geometry specimens equals to 28.22. B and W are the width and length of the specimen, respectively [34].

The aim of this work is evaluation of bonding strength and interfacial fracture toughness of 316L S.S plasma sprayed coating on aluminum substrate using three different methods referred as tensile adhesion test, four-point bending test and modified chevron-notched short-bar (SB) test.

II. Experimental Procedure

A. Materials and Coating Process

The Sulzer-Metco 41C-NS stainless steel was used as coating material. The powder specifications are given in Table I [35]. After preparation of TAT, four-point bend and SB specimens from commercial pure (CP) aluminum slab, the desired surfaces for coating were firstly sand blasted using grit alumina particles ((Metcolite FA), Sulzer-Metco, Westbury, New York, USA) at a pressure of 414 kPa. The nozzle-specimen distance and nozzle-specimen angle were 50 mm and 90°, respectively. Subsequently, the specimens were blown with compressed air, rinsed and cleaned in alcohol. The roughness of surfaces was determined using Surfometer (series 400, System Operating Instructions Precision Devices, Inc. Michigan, USA). The measured surface roughness, R_a, was in the range of 4-6 μm. The coating material was deposited on substrate using Sulzer-Metco plasma spray equipment. The plasma spraying conditions are specified in Table II. The particle impact conditions were monitored with the DPV 2000 system [36]. The thickness of applied coating was measured by micrometer of optical microscopy in different regions of each specimen. Eventually, mean value was considered as coating thickness of specimen. The porosity percentage and mean pore size were determined for each specimen using Clemex analyzer software.

B. Specimens Preparation

1. Tensile Adhesive Test (TAT) Specimen

The tensile adhesive tests were conducted according to ASTM C633 test method [14]. The support fixture having a contact diameter of 24.80 mm against the coated specimen was manufactured from mild steel (see Fig. 1). The FM 1000 polyamide-epoxy adhesive thin film from Cytec Industries Inc., New Jersey, was selected as binder. The adhesive specifications, according to manufacturer data sheet are given in Table III [37]. During the curing cycle, an alignment fixture was used to hold the coating surface and bonding portion of the support fixture precisely in a parallel orientation. In order to minimize adhesive penetration into the coating during curing, the coating facing were placed downwards. Tensile tests were conducted by using an Instron 1331 universal machine with adaptors designed to grip and transfer loads to the specimens. The schematic configuration of tensile adhesion test is given in Fig. 2 [38]. To minimize shear forces at interface or within the coating, a universal joint from the load cell was employed as a self-aligning mechanism. The specimens were pulled in tension with crosshead speed of 0.01 mm/min. The maximum load value was determined from load-time curve and bond strength was calculated by dividing the peak load to the cross-sectional area of the specimen. The maximal stress exerted at the coating-substrate interface never exceeded the rupture stress of the adhesive used.

TABLE I
THE SPECIFICATIONS OF SULZER-METCO 41C-NS COATING POWDER [35]

Powder Designation	Sulzer Metco 41C-NS
Chemistry, wt.%	Fe 17Cr 12Ni 2.5Mo 2.3Si 0.03C (similar to AISI Type 316L stainless steel)
Particle Size Range, μm (mesh)	-106 +45 (-140 +325)
Production Route	Water Atomizing
Processes	Air Plasma, Combustion Powder
Properties & Applications	Premium grade austenitic nickel-chrome stainless steel. Coatings can be easily machined. Recommended for cavitation and low temperature erosion resistance.

TABLE II
PLASMA SPRAYING CONDITIONS FOR COATING OF 41C-NS ON AL-SUBSTRATE

Arc Current, A	600
Arc Voltage, V	30
Flow Rate of Argon as Plasma Gas, l/min	70
Flow Rate of Particle Carrier Gas, l/min	3
Coating Powder Particles Feed Rate, g/min	8
Torch Distance from Specimen Surface, mm	50
Torch Angle with Specimen Surface, deg.	90

TABLE III
SPECIFICATIONS OF FM 1000 POLYAMIDE-EPOXY ADHESIVE THIN FILM [37]

Nominal Thickness (mm)	Shelf Life (months)	Curing Temp. (°C)	Curing Time (min)	Tensile Shear, psi (MPa)
0.075 to 0.360	6, at 30°C	175	60	7200 (49.64) at 24°C

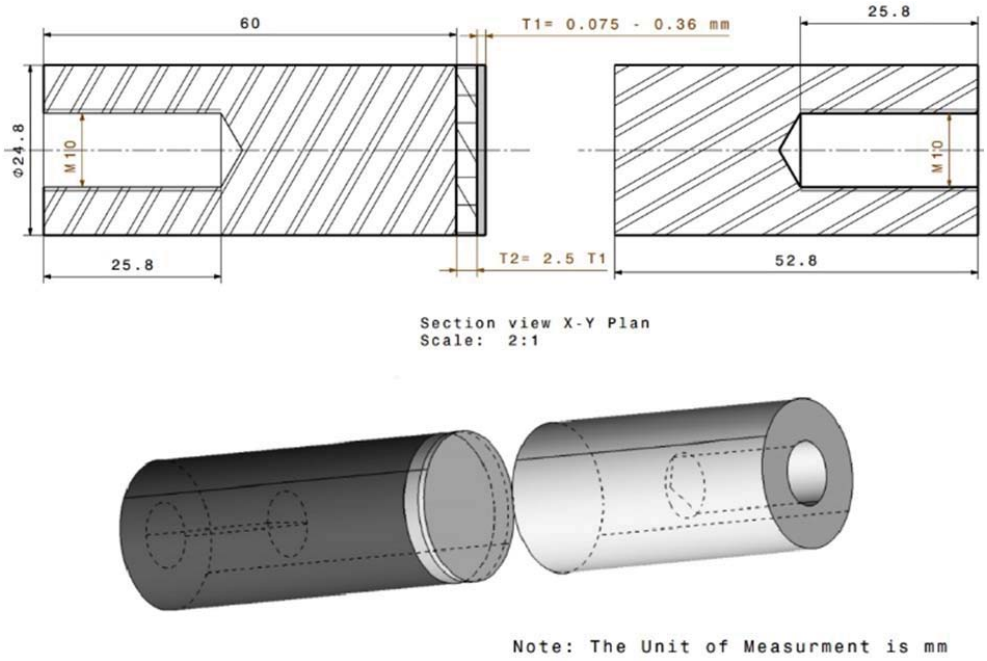

Fig. 1 Schematic illustration of the tensile adhesive test specimen's components

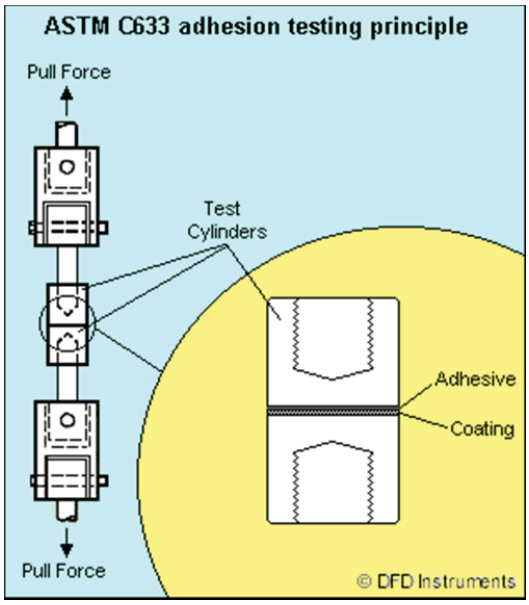

Fig. 2 Configuration of tensile adhesion test specified by DFD Instruments [38] according to ASTM C633

2. Four-Point Bending Test Specimen for Interfacial Fracture Toughness Determination

The four-point bending tests were performed on 316L S.S coated aluminum specimen with the dimensions of 50.00 mm × 3.80 mm × 2.00 mm. Fig. 3 shows the dimensions of the specimen. To provide reliable results, the test was repeated for five times. The coating thickness was in the range of 340-530 μm. Before loading, a notch was made through the thickness of the coating using a low speed diamond saw (see Fig. 4). The depth of notch was considered less than 2/3 coating thickness. The sides of the specimens were polished for optical microscopic examinations of notch zone. The microstructural observation of the tested specimen was carried out on optical microscope.

Four-point bending tests were conducted in an Instron 1331 universal machine. The crosshead speed was selected as 0.01 mm/min. This crosshead speed value can promote the required stable crack growth, whereas a fast loading rate could cause cracks to propagate unstably. Fig. 5 shows the special jigs which were used in order to minimize any possible bending moment. The utility of these jigs for four-point bending test corresponds to ASTM C1341 standard test method [39].

The list of material properties of 316L S.S coating and Al-substrate, which are needed for calculation of interfacial fracture toughness, are given in Table IV. Dundurs' parameter, β, has been calculated corresponding to (7) using the material properties.

3. Modified Chevron-Notched Short-Bar Specimen for Interfacial Fracture Toughness Determination

In this study, four parts of a modified chevron-notched short-bar specimen were machined from aluminum slab (Figs. 6 and 7). The dimensions of specimen were mostly consistent with those of the standardized homogeneous short-bar specimen presented in ASTM E1304. After grit blasting and cleaning the chevron shaped region, the strongly bonded coating with the thickness in the range of 250-300 μm was provided on this section. The deposition parameters are same as those which have been indicated in Table I. The region between front face and Chevron notch (10.50 mm) and the surrounding area were covered with lubricant to produce a weekly bond coating (see part 2 in Fig 6). With the use of FM 1000 polyamide-epoxy adhesives and the third part, as the roughened and mating part, the short bar specimen configuration would be completed entirely. The part 4, as a pin,

provides the integrity of parts 1 and 2. During curing, all specimens were also assembled with the coating facing downwards to minimize adhesive penetration into the coatings. To provide a good statistical sampling of the interfacial properties, five specimens were tested and analyzed using such modified chevron-notched short-bar specimen.

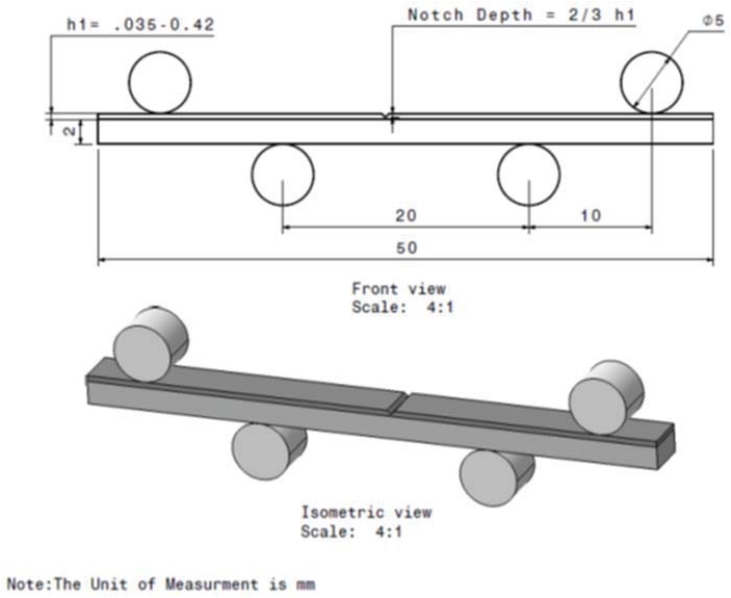

Fig. 3 A schematic illustration of the four-point bending specimen dimensions and notch created by diamond saw

Fig. 4 Optical micrograph, showing the shape of notch which has made through the thickness of the coating using a low speed diamond saw, X100

TABLE IV
LIST OF MATERIAL PROPERTIES OF 316L S.S COATING AND AL-SUBSTRATE

Mechanical Properties	316L S.S-Coating	Al-Substrate
Elastic Modulus, E (GPa)	193	69
Poisson's Ratio, ν	0.30	0.33
Shear Modulus, μ (GPa)	83	25
Dundurs Parameter, β:	0.126	

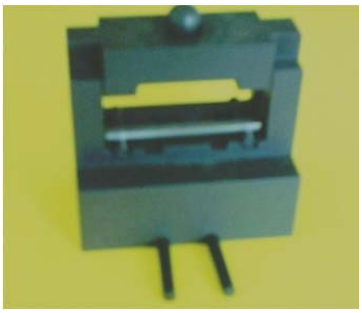

Fig. 5 The utilized jigs for four-point bending test, corresponding to ASTM C1341 standard test method

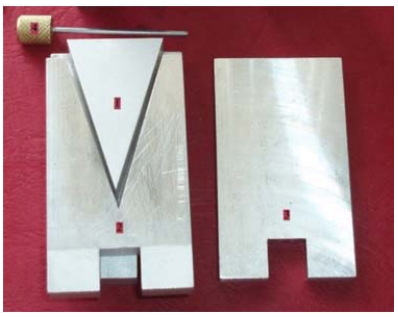

Fig. 6 Showing the modified chevron-notched short-bar specimen consisting of parts 1-4

III. RESULTS AND DISCUSSION

A. Particles Impact Conditions Throughout Coating

The particle impact conditions were monitored with the DPV 2000 system [36]. The particles' temperature, velocity, size and energy were measured every five seconds. The data

were provided along the centerline of the spray plum. A typical output from DPV 2000 system is illustrated in Fig. 8.

B. Microstructure Examination

Fig. 9 shows typical SEM image of 316L S.S coating on Al-substrate. The morphology of coating demonstrates lamellar nature of plasma sprayed coatings. Moreover, there are some porosities at the coating surface. The porosity percentage, mean pore length and width sizes at this typical coating surface were determined by using Clemex Software [40] as 17.35% (statistics: 903), 2.43 and 1.26 μm, respectively (see Fig. 10).

C. Mechanical Properties

1. Bonding Strength

The typical load-displacement curve driven from the tensile adhesion test is shown in Fig. 11. The maximum load value and cross-sectional area of the specimen were used for determination of bonding strength. After repeating the test for five times, the mean tensile bond strength value was calculated and given in Table V. The examination of fractured specimen surface indicates that failure has occurred basically inside the coating (cohesive type). However, the partial delamination (especially at the circumference of the specimen) has occurred at coating/adhesive- and coating/substrate- interfaces (Figs. 12 (a), (b)). This could be due to different stress conditions in such areas. The sz normal stress distribution in half of standard tensile adhesion test specimen is shown in Fig. 13. The magnitude of the stress represented by each contour for a given stress of 1 MPa can be realized from right y-axis. The zones I to IV denote to the part of the mild steel counter bar, adhesive, 316L SS coating and part of the Al-substrate, correspondingly.

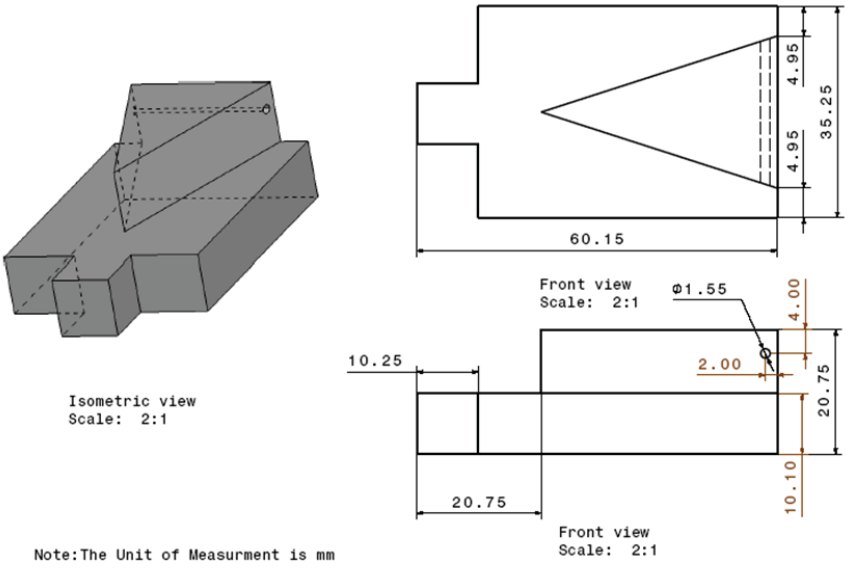

(a)

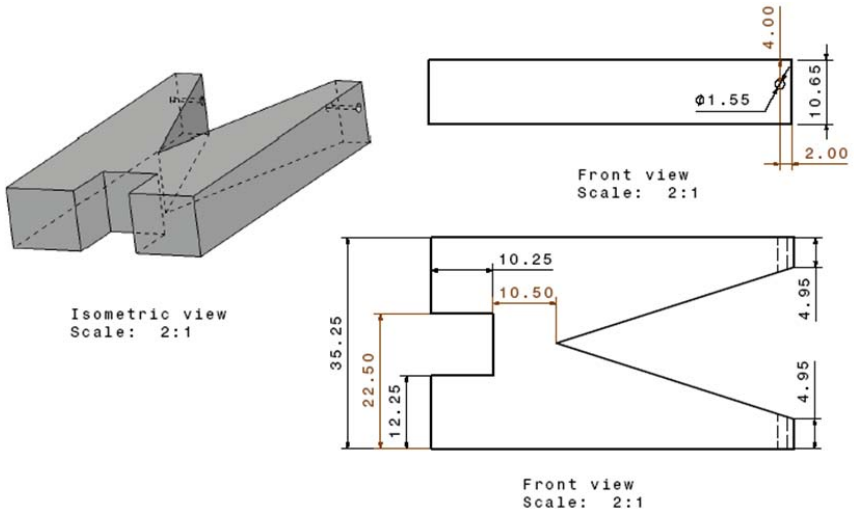

(b)

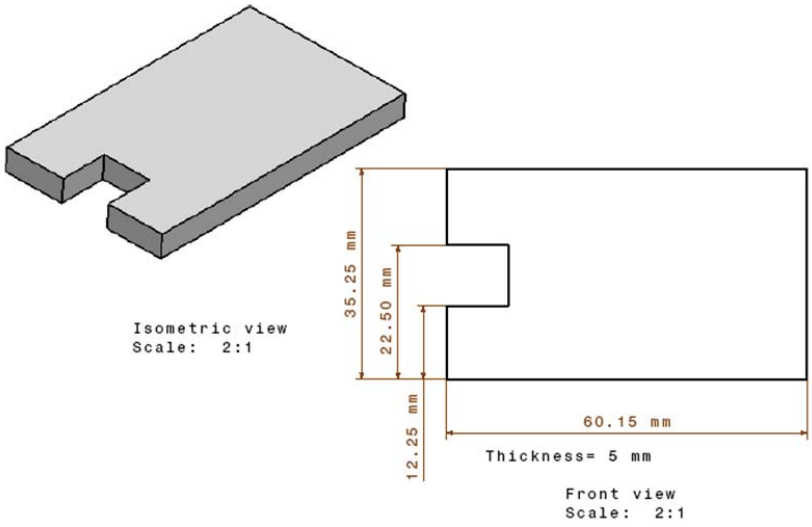

(c)

Fig. 7 The dimensions of modified chevron-notched specimen parts (a-c), in consistent with those of the standardized homogeneous short-bar specimen, presented in ASTM E1304

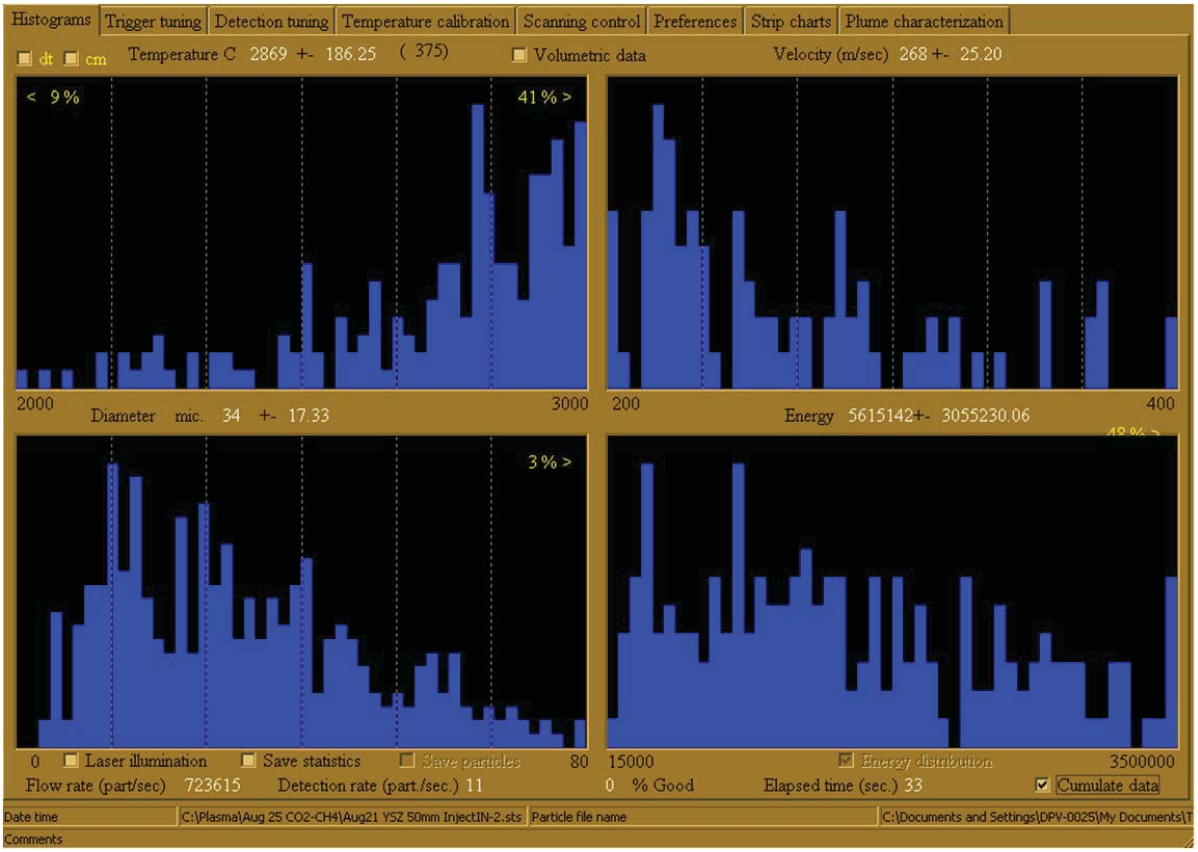

Fig. 8 A typical output from DPV 2000 system showing particle impact conditions

According to Babu et al. work results [41], the elastic or plastic properties mismatch of coating and substrate materials results in stress concentrations around the circumference near the interface. The magnitude of these stresses decreases from the circumference toward the center of specimen because of the increased triaxiality. The specimen preparation procedure is also important factor in specimen failure mechanism. Furthermore, the residual stresses in particular coated part with specific shape could be different from those of the test specimen [12]. Therefore, the determined bonding strength value cannot be considered as a stress value which can be sustained with an actual specimen in service condition.

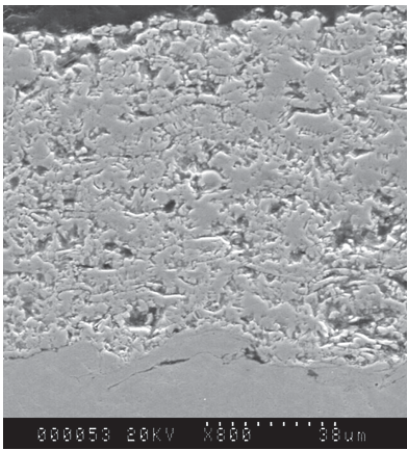

Fig. 9 SEM image of 316L S.S coating on Al-substrate

2. Interfacial Fracture Toughness: Results From Four-Point Bending Test

Due to loose contact points, at the beginning of the test, the system needed to adjust itself. As the load built up, it raised to the maximum point. The load of the delamination was determined by the load at which a sharp load drop occurred. Hence, this point is recorded as the maximum load sustained by the coating. Subsequently, load tended to get constant signifying the beginning of load bearing via plastic deformation of the substrate material. The examination of test specimen sides after bending test indicated that the loading caused cracks initiation around the notch as shown in Fig. 14. The main crack was propagated through entire coating thickness to reach coating/substrate interface which resulted in coating delamination along the interface.

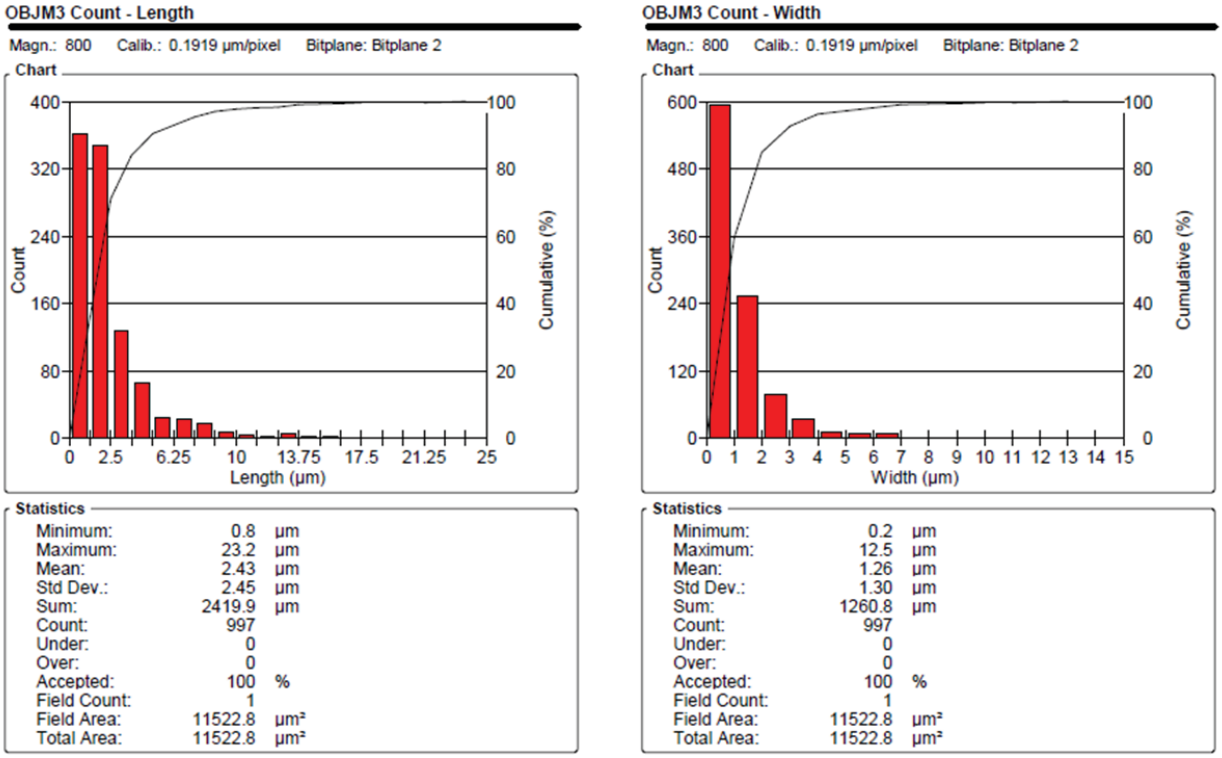

Fig. 10 Pore length and width size analysis at a typical coating surface, using Clemex Software.

TABLE V
THE RESULTS OF TESTS WHICH WERE CARRIED OUT IN CORRESPONDING WITH ASTM STANDARD TEST METHODS

Test specimen Designation	No. of Tests	Coat Thick. (µm)	Max. Load avg. (N)	σ (MPa)	M (N.m/m)	G_{ss} (J/m^2)	K_{IC} (MPa√m)	K[a], (MPa√m)
TAT	5	390-615	9260±1036	19.16±2.14	—	—	—	—
4-Point Bending	5	360-500	114.16±1.18	—	150.21±0.91	33.12±2.55	7.96±0.26 [a]	3.70±0.14[b]
SB	5	350-450	439.06±73.59	—	—	—	1.56±0.26 [c]	—

a. The interfacial fracture toughness calculated using (9).
b. Complex stress intensity factor calculated using (1)-(7) and assumption of interfacial crack propagation occurs when the strain energy release rate, G_{ss}, equals to the critical energy release rate, G_c, of the interfacial failure.
c. The interfacial fracture toughness calculated using (10).

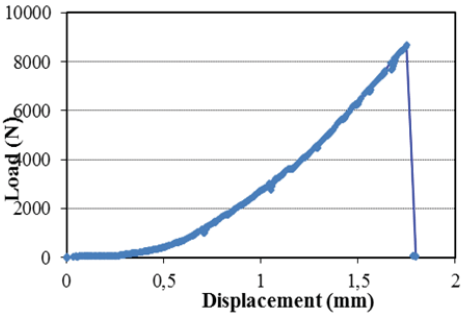

Fig.11 Typical load-displacement curve of tensile adhesion test

(a)

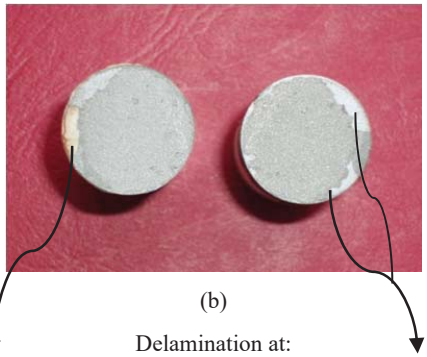

(b)

Delamination at:
coating/adhesive-interface coating/substrate-interface

Fig. 12 The fractured specimen surface showing, (a) failure basically inside the coating (cohesive type) and (b) partial delamination at coating/adhesive- and coating/substrate-interfaces

The critical bending moment, M, corresponding to the delamination load was computed by using (1) (see Table V). Considering the coating and specimen thickness values, as well as the given data in Table IV, the Dundurs' Parameter, β, and strain energy release rate, G_{ss}, values were calculated using (7) and (2). Since interfacial crack propagation occurs when the strain energy release rate, G_{ss}, equals to the critical energy release rate, $G_{c,}$ of the interfacial failure, the stress intensity factor, as a complex form by stress fields near the crack tip, was calculated by setting G_{ss}=G_c. Therefore, by considering (2)-(7), the complex stress intensity factor has been calculated and reported in Table V. As it can be recognized, for calculation of the strain energy release rate, the measurement of crack length is unnecessary for the four-point bend test configuration. As suggested by other researchers, the four-point bend test is a successful technique to evaluate the properties of interface between dissimilar materials [5], [7], [8], [19]-[23]. Considering Dundurs [42] statement, in the case of the crack propagation along the interface between two dissimilar materials just due to a mismatch in their elastic properties, there is a mode-mixity effect. Therefore, interfacial fracture mechanics should be used to describe crack growth along the interface between two dissimilar isotropic materials [43].

It should be noted that the computed value of fracture toughness in the present study is based on the assumption that the sample undergoes bending as well as tension. Thus, complex form by stress fields near the crack tip has been considered for calculation of fracture toughness, whereas the fracture toughness values in literature are quoted for mode I failure. This might be the reason of discrepancies between the calculated and reported fracture toughness values of materials used in present work.

3. Interfacial Fracture Toughness: Results From Modified Chevron-Notched Short-Bar Specimen

A typical smooth load-displacement curve in Fig. 15, which is resulted from modified chevron-notched short-bar specimen testing, indicates the stable crack growth before final failure. With the assumption that the modified and homogeneous short-bars displays the same compliance behavior, the fracture toughness was calculated by using (10) and reported on Table V. The value is lower than that of predicted from bending test. Referring to Charreyron et al. [44], aside from the obvious differences in elastic properties of the materials on either side of the interface (which is the basis of the most complex stress intensity theory), there is also potentially significant shear (Mode II) loading arising from the thermal expansion mismatch between the plasma-sprayed coating and the metal substrate. The interfacial fracture toughness would be also influenced by stress conditions. For a meaningful evaluation of coating and substrate interfacial fracture toughness, any effect of plasma-sprayed parameters alternation on mechanical integrity of the coating/substrate interface should be taken into account.

The calculated fracture toughness value reported in this study cannot be taken as absolute value, because a proper confirmation of the minimum stress intensity coefficient, Y_m^*, value for modified chevron-notched short-bar Specimen is required.

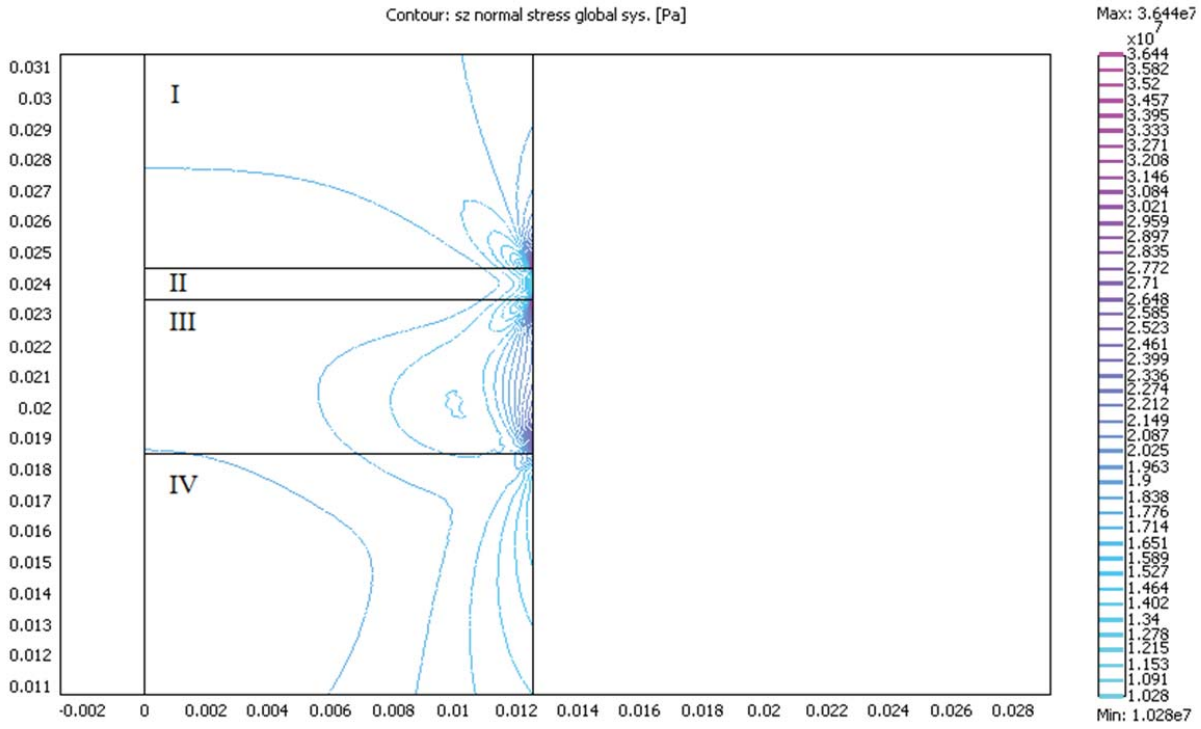

Fig. 13 Showing the ″<sigma> z″ (sz) normal stress distribution in standard tensile adhesion test for a given stress of 1 MPa.

Fig. 14 Optical micrograph of many cracks around saw notch and crack propagation through the coating/substrate interface, X100

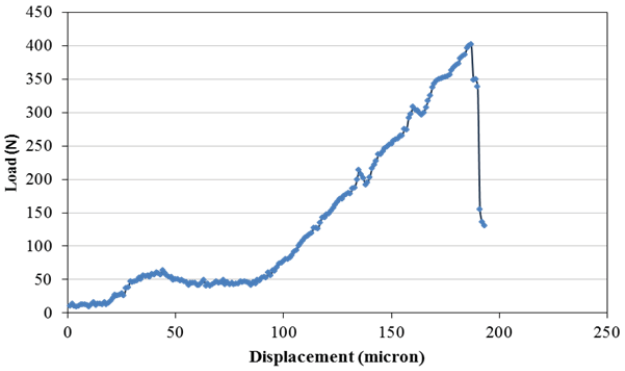

Fig. 15 Typical load-displacement curve resulted from modified chevron- notch specimen testing

IV. Conclusion

- It is concluded that a proper bonded coating of 316L S.S. on aluminum could be produced by plasma spray processing.
- TAT results can be utilized for as quality control and developing thermal spray coatings with improvement adhesion and integrity.
- The determined bonding strength value based on TAT cannot be considered as a stress value which can be sustained with an actual specimen in service condition.
- The four-point flexure test which is based on the storage of a specific amount of elastic energy on bending and a release of this energy on fracture is a successful technique to evaluate the properties of interface between dissimilar materials.
- The calculated fracture toughness value reported for modified chevron- notch specimen testing cannot be taken as absolute value.

Acknowledgment

The authors wish to express their thanks to center for advanced coating technologies of university of Toronto for providing laboratory equipment utilized in this study. Special thanks to Dr. Larry Pershin to help plasma spraying of specimens. The authors wish to thank also Mr. Tiegang Li at laboratories of center for his kind assistance to set up the equipment and preparing the specimens to carry out the tests.

References

[1] R.B. Heimann, "*Plasma Spray Coating", Principles and Applications*", VCH, 1996.

[2] L. Pawlowski, "*The Science and Engineering of Plasma Spray Coatings*", Wiley on line library, 1995.
[3] R. Krebs, B. Stiebels, L. Spiegel, E. Pott, "FSI-Ottomotor mit Direkteinspritzung im Volkswagen Lupo", Fortschritt-Berichte, Wiener Motorensymposium, VDI, 12, 2000, p. 420.
[4] K. U. Kainer. "*Metal Matrix Composites: Custom-Made Materials for Automotive and Aerospace Engineering*", Copyright Weinheim: Wiley-Vch Verlag GmbH & Co. KGaA, 2006.
[5] J.H. Kim, S.B. Lee, "Stress intensity factors and crack initiation directions for ceramic/metal joint", *Theoretical and Applied Fracture Mechanics*, 30, 1998, pp. 27-38.
[6] M. Van Den Burg, J.Th.M. De Hosson, "Mechanical performance of metal-ceramic interfaces produced by laser processing", *Interface Science*, 3, 1995, pp. 107-118.
[7] W. Lee, "Strength of Si 3 N4 /Ni-Cr-Fe alloy joints with test methods: Shear, tension, three-point and four-point bending", *J. of Materials Science*, 32, 1997, pp. 6657-6660.
[8] Q. Ma, "A four-point bending technique for studying subcritical crack growth in thin films and at interfaces", *J. of Materials Research*, 3, 12, 1997, pp. 840-845.
[9] G.H. Heintze, R. Mc Pherson, "Fracture toughness of plasma-sprayed zirconia coatings", *Surface and Coating Technology*, 34, 1988, pp. 13-23.
[10] G.H. Heintze, R. Mc Pherson, "Further study of fracture toughness of plasma-sprayed zirconia coatings", *Surface and Coating Technology*, 36, 1988, pp. 125-132.
[11] M. Arrigoni, S. Barradas, M. Braccini, M. Dupeux, M. Jeandin, M. Boustie, C. Bolis, L. Berthe, "A comparative study of three adhesion tests (EN 582, similar to ASTM C633, LASAT (Laser Adhesion Test), and bulge and blister test) performed on plasma sprayed copper deposited on aluminum 2017 substrates", *J. Adhesion Sci. Technology*, 5, 20, 2006, pp. 471-487.
[12] G. Qian, T. Nakamura, C.C. Berndt and S.H. Leigh, "Tensile toughness test and high temperature fracture analysis of thermal barrier coating", *Acta Matereralia*, 45, 4, 1997, pp. 1767-1784.
[13] D. Rickerby, "Measurement of coating adhesion", in Metallurgical and Ceramic Protective Coatings", K.H. Stern Ed. Chapman & Hall, London, 1996, pp. 306-333.
[14] ASTM C633-01, "Standard test method for adhesion or cohesion strength of thermal spray coatings", 2001.
[15] M. J. Filiaggi, R. M. Pilliar, "Mechanical testing of plasma-sprayed ceramic coatings on metal substrates: Interfacial fracture toughness and tensile bond strength" *J. of Materials Science*, 26, 1991, pp. 5383-5395.
[16] A. G. Evans, J. W. Hutchinson, "Effects of non-planarity on the mixed mode fracture resistance of bimaterial interfaces", *Acta Metallurgica*, 3, 37, 1989, pp. 909-916.
[17] A. G. Evans. M. Riihle. B. J. Dalgleish, P. G. Charalambides. "The fracture energy of bimaterial interfaces", *Materials Science and Engineering A*, 126, 1990, pp. 53-64.
[18] R. Mc Pherson, "Metallurgical and protective coatings: The relationship between the formation, microstructure and plasma sprayed coatings", *Thin Solid Films*, 83, 1981, pp. 297-310.
[19] E. Hanus, T. Ericsson, "Influence of four-point bending fatigue on the residual stress state of a pressure-rolled particulate reinforced metal matrix composite", *Materials Science and Engineering A*, 194, 1995, pp. 147-156.
[20] L. R. Katipelli, A. Agarwal, N. B. Dahotre, "Interfacial strength of laser surface engineered TiC coating on 6061 Al using four-point bend test", *Materials Science and Engineering A*, 289, 2000, pp. 34-40.
[21] Q.S. Yang, X.R. Peng, A.K.H. Kwan, "Strain energy release rate for interfacial cracks in hybrid beams", *Mechanics Research Communications*, 33, 2006, pp.796-803.
[22] J.W. Hutchinson, Z. Suo, "Mixed mode cracking in layered materials", *Advances in Applied Mechanics*, J. W. Hutchinson and T. Y. Wu, Eds. Academic Press, 29, 1992, pp. 63-191.
[23] R. Rice, "Elastic fracture mechanics concept for interfacial cracks", *Journal of Applied Mechanics*, 55, 1988, pp. 98-103.
[24] A. Strawbridge, H.E. Evans," Mechanical Failure of thin Brittle Coatings", *Engineering Failure Analysis*, Vol.2, 2, 1995, pp. 85-103.
[25] LM. Barker, "A Simplified Method for Measuring Plane Strain Fracture Toughness", *Engineering. Fracture Mechanic*, 9, 1977, pp. 361-369.
[26] LM. Barker, "Compliance Calibration of a Family of Short Rod and Short Bar Fracture Toughness Specimens", *Engineering. Fracture Mechanic*, 17, 1983, pp. 289-312.
[27] D. Munz, RT. Bubsey, J.E. Srawley, "Compliance and stress intensity coefficients for short bar specimens with chevron notches". *Int. J. of Fracture*, 16, 1980, pp. 359-374.
[28] LM. Barker, "Short Bar Specimens for K_{Ic} Measurement", in Fracture Mechanics Applied to Brittle Materials ASTM STP 678, S.W. Freiman, Ed. American Society for Testing and Materials, 1979, pp. 73-82.
[29] J. Nakayama, "Direct measurement of fracture energies of brittle heterogeneous materials". *J Am. Ceram. Society*, 48, 1965, pp. 583-587.
[30] R.T. Bubsey, D. Munz, W.S. Pierce, J.L. Shannon, "Compliance calibration of the short rod chevron-notch specimen for fracture-toughness testing of brittle materials". *Int. J. of Fracture*, 18, 1982, pp. 125-133.
[31] JJ. Jr. Mecholsky, L.M. Barker, "A chevron-notched specimen for fracture toughness measurements of ceramic-metal interface", Chevron-Notched Specimens: Testing and Stress Analysis. ASTM STP 855, 1984, pp. 325-336.
[32] Jr. JC., Newman, "A review of chevron-notched fracture specimens", Chevron-notched specimens: Testing and stress analysis. ASTM STP 855, 1984, pp. 5-31.
[33] D. J. Lee, "Simple method to measure the crack resistance of ceramics materials", *J. of Materials Science*, 30, 1995, pp. 4617-4622.
[34] ASTM E 1304-97, "Standard test method for plane-strain chevron-notch fracture toughness of metallic materials", 2002 pp. 1-11.
[35] Sulzer Metco, "Thermal spray materials guide", 2012.
[36] L. Pouliot, J. Blain, F. Nadeau, DPV-2000 reference manual, Tecnar Automation Ltd, Montreal, 1999.
[37] "FM 1000 Adhesive Film", Cytec Engineered Materials, Technical Product description, Report No. 120502, pp. 1-9.
[38] www.dfdinstrument.com
[39] ASTM C1341-00, Standard test method for flexural properties of continuous fiber reinforced advanced ceramic components", pp. 518-536.
[40] http://www.metlabcorp.com/pdf/ClemexVisionLite.pdf
[41] M. V. Babu, R.K. Kumar, O. Prabhakar, N.G. Shankar, "Fracture mechanics approaches to coating strength evaluation", *Engineering Fracture Mechanics*, 55, 1996, pp. 235-248.
[42] J. Dundurs, "Edge-Bonded Dissimilar Orthogonal Elastic Wedges", *J. Appl. Mech*., 36, 1969, 650-652.
[43] A. A. Volinsky, D.F. Bahr, M.D. Kriese, N.R. Moody, W. Gerberich, "Nanoindentation methods in interfacial fracture testing" in "Interfacial and nanoscale failure", vol.8., W. Gerbrich, W. Yang, Vol. Eds. from "Comprehensive Structural Integrity, Fracture of Materials From Micro to Nano" vols.1-10, I. Milne, R. O. Ritchie, B. Karihaloo, Eds.-in-Chief, New York: Elsevier Pergamon, 2003, pp. 453-493.
[44] P. O. Charreyron, N. J. Bylina, J. G. Hannoosh, in "Fracture Mechanics of Ceramics", Vol. 8, edited by R. C. Bradt, A. G. Evans, D. P. H. Hasselman and F. F. Lange, Plenum Press, New York, 1986, pp. 225-250.